epithelium. However, to the best of our knowledge, there are no reports on whether CK expression patterns can be used to distinguish between primary lung SCC and metastatic lung SCC from another organ. We determined that primary lung SCC can be differentiated from metastatic lung SCC of the tongue by analyzing their CK expression pattern.

METHODS

Patients and materials

Between 1977 and 2008, 17 patients with histories of surgical treatment for tongue SCC underwent surgery for lung SCC at our hospital. Since it was unknown whether each of these lung tumors was a primary tumor or a metastasis from the tongue, we termed these patients the 'unknown group'. Seventeen lung SCC and 15 primary tongue SCC tumors (specimens of two cases were not available) were obtained from the unknown group. Additionally, 26 patients who underwent surgery for primary lung SCC at the same hospital in 1998 without a history of any other cancer were selected randomly for comparison. Since the tumors of the latter group were definitely primary lung cancers, we termed these patients the 'definite primary group.' Tumor specimens were obtained from all 26 patients in this group. This study was performed with informed consent and followed the guidelines for experimental investigation with human subjects required by the institution.

At first, we classified the lung tumors of the unknown group (Cases 1–17) into three subgroups, metastatic, primary or unclassified. Traditionally, these diagnoses are based on clinicopathological findings, such as tumor location, number of lesions or pathological comparisons with the putative primary tumor. But this approach does not always give a definite diagnosis. Therefore, we made the diagnoses considering prognosis after lung surgery as well. The criteria used in this study are shown in Table 1. Fifteen cases were classified as metastases or primaries in a mutually exclusive manner. The other two cases remained unclassified by these criteria. The diagnostic procedures are summarized in Table 2. Cases 8–11 satisfied only one metastasis criterion. In fact, Cases 8–10 died within one year of resection of their lung tumors, which was relatively soon for surgical cases of primary lung SCC. Case 11 was 23 years old at the time the lung tumor developed, which was very young for primary lung SCC. None of Cases 8-11 satisfied any of the five primary items. Thus, they were considered metastases of tongue SCC. The lung tumor of Case 14 had extensive *in situ* spreading. The lung tumor of Case 15 was centrally located. Additionally, neither Case 14 nor Case 15 satisfied any criteria characteristic of a metastasis. Thus, they were considered likely primary lung tumors. Case 16 and Case 17 showed both primary and metastatic characteristics, and so they remained unclassified. In total, 11 lung tumors from the unknown group were diagnosed as metastatic lung SCC.

Table 1 Diagnostic criteria for squamous cell carcinoma (SCC) observed in the unknown group

Pro metastasis findings
(1) Multiple lung lesions of similar size were present.
(2) Survival time after removal of the lung tumor was less than 6 months.
(3) Histological features favored a metastasis (i.e. similar cellular appearance in both lung and tongue SCC or exceeding central necrosis in the lung tumor).

Pro primary findings
(4) Pathological N0 of the tongue SCC was proved.
(5) *In situ* carcinoma was seen in the lung tumor.
(6) The tongue SCC had been controlled for more than 2 years before the emergence of a lung tumor.
(7) Survival time after removal of the lung tumor was more than 3 years.
(8) The site of the lung lesion was central (i.e. in the main, lobular or segmental bronchus).

N0, no metastasis to lymphnodes.

Table 2 Final tumor classification results (metastatic, primary or unclassified) for the unknown group

Case	Satisfied diagnostic criteria†		Diagnosis
	pro metastasis	pro primary	
1	(1), (3)	None	Metastasis
2	(1), (2), (3)	None	Metastasis
3	(2), (3)	None	Metastasis
4	(2), (3)	None	Metastasis
5	(2), (3)	None	Metastasis
6	(2), (3)	None	Metastasis
7	(2), (3)	None	Metastasis
8	(3)	None	Metastasis
9	(3)	None	Metastasis
10	(3)	None	Metastasis
11	(3)	None	Metastasis
12	None	(5), (6), (7), (8)	Primary
13	None	(4), (5)	Primary
14	None	(5)	Primary
15	None	(8)	Primary
16	(3)	(7)	Unclassified
17	(1)	(4)	Unclassified

†See Table 1 for definitions of the diagnostic criteria.

Immunohistochemistry

The specimens were prepared from formalin-fixed, paraffin-embedded tissue blocks. The primary antibodies used in this study are listed in Table 3. CK5/6 reacts with CK5 and CK6, which are high molecular weight keratins that are expressed in squamous epithelium. CK7 and CK19 are relatively low molecular weight CK expressed in columnar epithelium, and they are not normally expressed in stratified squamous epithelium. CAM5.2, which has primary reactivity with CK8 and weaker but distinct reactivity with CK7, reacts with most

Table 3 Antibodies for cytokeratins used in this study

Antibody	Source	Clone	Dilution	HIER
CK5/6	Chemicon Illinois, USA	D5/16B4	1:100	In citrate (pH 6.0)
CK7	Progen Heidelberg Germany	OVTL12-30	1:50	In Tris-EDTA (pH 9.0)
CAM5.2	Becton-Dickinson San Jose, CA, USA	CAM5.2	prediluted	In Tris-EDTA (pH 9.0)
CK19	Dako Glostrup, Denmark	RCK108	1:20	In citrate (pH 6.0)
p63	Thermo-Scientific Fermont, CA, USA	4A4	1:100	In citrate (pH 6.0)

HIER, heat-induced epitope retrieval.

Table 4 Clinicopathological characteristics of examined patients with definite primary or unknown lung squamous cell carcinomas. For final diagnosis of the unknown group, see Table 2 and text

Group	Definite primary		Unknown	
Final diagnosis	Primary ($n = 26$)	Metastasis ($n = 11$)	Primary ($n = 4$)	Unclassified ($n = 2$)
Age				
Mean (years)	69.0	46.3*	61.8	46.0
Sex				
Male/Female	22/4	6/5	4/0	1/1
Smoking index†				
Mean	1287	396*	1298	630
Differentiation				
W/M+P	3/23	7/4*	2/2	0/2
Size of lung tumor				
Mean (mm)	50.2	38.6	47.3	23.5
Location of lung tumor				
Peripheral/Central	18/8	11/0	2/2	2/0
Stage of lung tumor				
I/II + III	13/13	2/9	2/2	1/1

*$P < 0.01$. P-values for comparisons between the definite primary group and the unknown group (P-values for age, smoking index and tumor size were obtained by Welch's t-test and those for sex, tumor site, differentiation and stage were obtained by chi-squared test).

†Smoking index, a product of the numbers of cigarette per day and duration (years).

W, well differentiated; M+P, moderately or poorly differentiated.

epithelial cells with the exception of stratified squamous epithelium.[8,9] p63, a nuclear transcription factor predominantly expressed in stratified epithelium,[10] was also evaluated. After deparaffinization, the sections were submerged in either sodium citrate buffer or Tris-EDTA buffer for heat-induced epitope retrieval at 97°C for 40 min. The immunostaining was carried out using the EnVision+ dextran polymer kit (Dako, Glostrup, Denmark) in Dako Autostainer (Dako, Glostrup, Denmark). Immunoreactivity was regarded as positive when 10% or more of tumor cells were stained.

Statistical analysis

Statistical analyses for correlation of clinicopathological features were performed by the chi-squared test and Welch's t-test. Statistical analyses for immunoreactivity were performed by the chi-squared test. Differences at $P < 0.05$ were regarded as significant.

RESULTS

Clinicopathological characteristics of patients examined

The patient characteristics are shown in Table 4. Compared with the definite primary group, cases of the unknown group whose lung tumors were diagnosed as metastases showed significantly younger onset, lower cumulative smoking and a higher proportion of well-differentiated tumors. On the other hand, primary tumors of the unknown group showed quite similar characteristics to the definite primary group: older age and high cumulative smoking history.

Immunohistochemical results

CK were localized to the cytoplasm and along the cell membrane. The staining of CK5/6 was strong and widely distributed both in tumor and in normal squamous cells. Staining of

Table 5 Positive ratio of each cytokeratin and p63 in the definite primary group and the unknown group

Group	Definite primary		Unknown		
Tumor site			Lung		
Diagnosis	Lung	Metastasis	Primary	Unclassified	Tongue
CK5/6	26/26	10/11	3/4	2/2	15/15
CK7	4/26	0/11	2/4	0/2	1/15
CAM5.2	21/26	1/11*	2/4	1/2	5/15*
CK19	20/26	2/11*	2/4	0/2	2/15*
p63	25/26	9/11	3/4	2/2	12/15

*$P < 0.01$. P-values for comparisons between the definite primary group and the unknown group (obtained by chi-squared test).

CK7, CAM5.2 and CK19 was observed in tumor cells as well as in normal bronchial epithelium, but not in normal squamous epithelium. In tumor cells, reactions were mainly observed in non-keratinized components. p63 staining was observed in the nuclei of tumor cells and normal squamous epithelial cells. Staining patterns of p63 were similar between primary tongue carcinomas and their metastases to the lung.

The frequency of the CK- and p63-positive tumors in each group is shown in Table 5. The expression of CAM5.2 in the lung SCC of the definite primary group (21 of 26, 81%) was significantly higher than in the primary SCC of the tongue (5 of 15, 33% ($P = 0.002$)) or the metastatic lung SCC (1 of 11, 9% ($P < 0.001$)). Also, the expression of CK19 in lung SCC of the definite primary group (20 of 26, 78%) was significantly higher than in the primary tumors of the tongue (2 of 15, 13% ($P < 0.001$)) or in the metastatic lung SCC (2 of 11, 18% ($P = 0.003$)). Representative images of tumors immunostained with CAM5.2 and CK19 are shown in Fig. 1. There are two types of primary SCC of the lung based on location, peripheral and central. However, we found no difference of reactivity of CAM5.2 and CK19 in the central and peripheral tumors. In fact, for CAM5.2 the positive frequency in central and peripheral types was 6 of 8 and 15 of 18, and for CK19 that was 6 of 8 and 14 of 18, respectively, which were not significantly different.

In all SCC CK5/6 and p63 were expressed very frequently and CK7 was rarely expressed. For distinguishing between primary tumors and metastases, the use of CAM5.2 and CK19 provided 81% and 78% sensitivity and 91% and 82% specificity, respectively. Both CAM5.2 and CK19 tended to be expressed more often in basal and parabasal tumor cells, which showed minimal squamous differentiation, than in upper layer cells or keratinizing cells. This was the case for both primary lung and tongue tumors and metastatic tumors. In other words, the two CK tended to be positive in basal or poorly-differentiated components, and to be negative in well-differentiated components.

Details of CAM5.2 and CK19 expression in the 11 metastatic tumors are listed in Table 6. The expression patterns were consistent in 90% (9/10) for CAM5.2 and 70% (7/10) for CK19, indicating relatively consistent expression patterns before and after metastasis.

DISCUSSION

When a lung SCC is detected in a patient with a history of tongue SCC, it may be difficult to make a distinction between a new primary tumor and a metastasis. Our results show that primary lung SCC express CAM5.2 and CK19 significantly more frequently than do metastatic lung SCC from the tongue, and CK are useful for differentiating between the tumor types. To the best of our knowledge, this is the first report to demonstrate the usefulness of CK expression patterns for distinguishing primary lung SCC from metastases.

To characterize CK profiles of metastatic lung SCC, we had to determine whether each of the lung tumors of the unknown group was primary or metastatic. We used the original criteria that include clinical course after lung surgery. Our criteria clearly identified 15 of 17 lung squamous tumors of the unknown group as primary or metastatic tumors. The patients who were diagnosed with metastases showed significantly younger ages of onset and lower cumulative smoking than the definite primary group. These characteristic features backed up our criteria, because tongue SCC patients are younger than those with primary lung SCC,[11–14] and because risk factors for tongue SCC include not only smoking but also alcohol intake, among other things.[12,15,16] Meanwhile, patients who were diagnosed with primary tumors showed similar characteristics to the definite primary group. These findings suggest that our criteria were largely appropriate. CAM5.2 and/or CK19 expression between primary and metastatic sites did not accord in three cases. The discrepancy may be due partly to heterogeneity of tumor cell characteristics. All tongue tumors in these three cases showed heterogeneous expression of CK. Specifically, two cases, judged as negative, included a small number of positively staining cells (<10%), and the other one, judged as positive, also had a negatively staining component (about 80%). Such components contradicting the final judgment might have metastasized to the lung.

CK, which are constituents of intermediate filaments of epithelial cells, are divided into at least twenty subtypes. The profile of CK expression differs depending on the epithelial cell type and the degree of cellular differentiation. We showed that primary lung SCC more frequently express

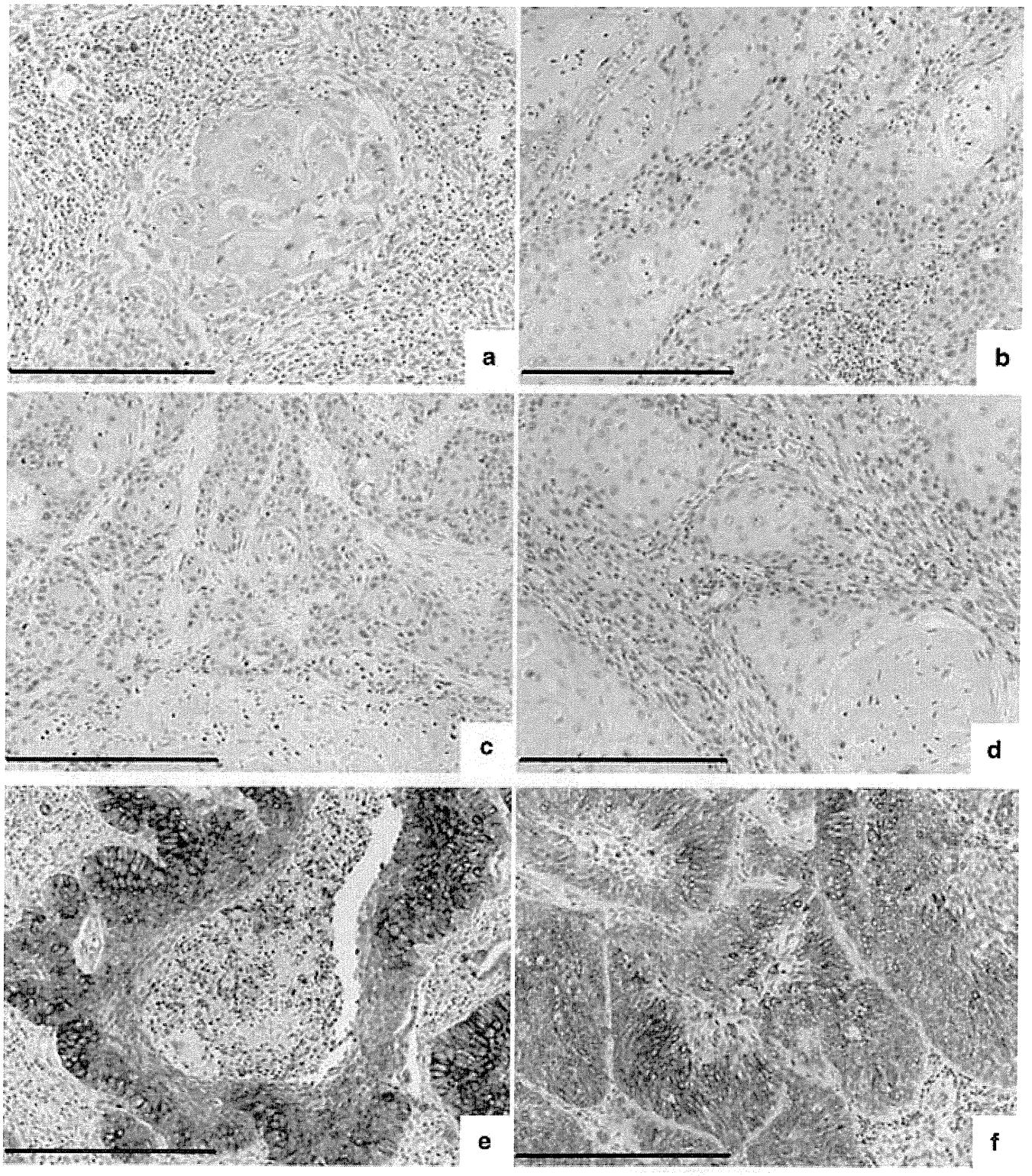

Figure 1 Representative images of squamous cell carcinoma (SCC) immunostained with CAM5.2 (**a,c,e**) and CK19 (**b,d,f**). A primary tumor of the tongue was negative for both cytokeratins (**a,b**). A metastatic lung SCC was also negative for both cytokeratins (**c,d**). Only a primary lung SCC expressed CAM5.2 (**e**) and CK19 (**f**). Scale bars, 300 μm.

Table 6 CAM5.2 and CK19 expression in primary and metastatic sites of tongue squamous cell carcinoma. Note that expression patterns were consistent in 90% (9/10) for CAM5.2 and 70% (7/10) for CK19

	CAM5.2			CK19		
Case	Tongue	Lung	Consistency	Tongue	Lung	Consistency
1	N/A	–	?	N/A	–	?
2	–	–	Yes	–	+	No
3	–	–	Yes	–	–	Yes
4	–	–	Yes	–	–	Yes
5	+	–	No	+	–	No
6	–	–	Yes	–	–	Yes
7	–	–	Yes	–	–	Yes
8	–	–	Yes	–	–	Yes
9	+	+	Yes	–	–	Yes
10	–	–	Yes	–	–	Yes
11	–	–	Yes	–	+	No

–, negative; +, positive; ?, unknown; N/A, not applicable.

CAM5.2 and CK19, CK of columnar epithelium, than primary tumors of the tongue and their metastases. There are two previous reports that are largely in line with our results. The first showed that CK8, 18 and 19, which are characteristic of columnar epithelium, were more frequently expressed in primary SCC of the lung and cervix than in SCC arising from various organs of proper squamous epithelium.[6] The second demonstrated that primary lung SCC express CK19 more frequently and intensely than SCC of the oral cavity.[7] Hamakawa *et al.* reported a somewhat higher value of CK19 reactivity, about 50%, in oral SCC,[7] whereas ours was 2/11 (18%) to 2/15 (13%). This is the result of the generally high reactivity of CK19 in their study, that is 100% strong positivity in primary lung SCC. The high reactivity may be due to: (i) their use of a different antibody and a different augmentation method; (ii) admixture of oral SCC, including those of tongue, gingiva, pharynx and larynx; and (iii) a possible of lack non-cancerous controls. We believe our methods are appropriate for detecting heterogeneous reactivity in a tumor.

Our method is highly useful for resected materials, as mentioned above, and it is also applicable for biopsy specimens, provided that pathologists who use this method carefully evaluate the results. Although primary lung SCC frequently express CAM5.2 or CK19, some cases show heterogeneous expression of these markers. Thus, when only a small amount of lung tissue is available, CAM5.2 or CK19 negative studies of biopsy materials do not necessarily mean that the entire tumor is negative for these markers. In such a case, our method would not be helpful for the distinction. However, if a biopsy specimen expresses either CAM5.2 or CK19, the finding will strongly suggest that the lung tumor is a new primary one.

In summary, primary lung SCC express CAM5.2 and CK19 more frequently than do metastatic lung SCC from the tongue. The profiling of these CK could be useful for distinguishing between primary tumors and metastases.

ACKNOWLEDGMENTS

The authors thank Mr Motoyoshi Iwakoshi and Ms Tomoyo Kakita (Division of Pathology, JFCR Cancer Institute) for their technical assistance. There are no conflicts of interests regarding submission of this manuscript.

REFERENCES

1 Carvalho AL, Magrin J, Kowalski LP. Sites of recurrence in oral and oropharyngeal cancers according to the treatment approach. *Oral Dis* 2003; **9**: 112–18.
2 Taneja C, Allen H, Koness RJ, Radie-Keane K, Wanebo HJ. Changing patterns of failure of head and neck cancer. *Arch Otolaryngol Head Neck Surg* 2002; **128**: 324–7.
3 Calhoun KH, Fulmer P, Weiss R, Hokanson JA. Distant metastases from head and neck squamous cell carcinomas. *Laryngoscope* 1994; **104**: 1199–205.
4 Nagle RB, Moll R, Weidauer H, Nemetschek H, Franke WW. Different patterns of cytokeratin expression in the normal epithelia of the upper respiratory tract. *Differentiation* 1985; **30**: 130–40.
5 Ramaekers F, Huysmans A, Moesker O *et al.* Monoclonal antibody to keratin filaments, specific for glandular epithelia and their tumors. Use in surgical pathology. *Lab Invest* 1983; **49**: 353–61.
6 van Dorst EB, van Muijen GN, Litvinov SV, Fleuren GJ. The limited difference between keratin patterns of squamous cell carcinomas and adenocarcinomas is explicable by both cell lineage and state of differentiation of tumor cells. *J Clin Pathol* 1998; **51**: 679–84.
7 Hamakawa H, Bao Y, Takarada M, Fukuzumi M, Tanioka H. Cytokeratin expression in squamous cell carcinoma of the lung and oral cavity: An immunohistochemical study with possible clinical relevance. *Oral Surg Oral Med Oral Pathol Oral Radiol Endod* 1998; **85**: 438–43.
8 Makin C, Bobrow L, Bodmer W. Monoclonal antibody to cytokeratin for use in routine histopathology. *J Clin Pathol* 1984; **37**: 975–83.
9 Moll R, Franke W, Schiller D, Geiger B, Krepler R. The catalog of human cytokeratins: Patterns of expression in normal epithelia, tumors, and cultured cells. *Cell* 1982; **31**: 11–24.
10 Di Como CJ, Urist MJ, Babayan I *et al.* p63 expression profiles in normal and tumor tissues. *Clin Cancer Res* 2002; **8**: 494–501.
11 Effiom OA, Adeyemo WL, Omitola OG, Ajayi OF, Emmanuel MM, Gbotolorun OM. Oral squamous cell carcinoma: A clinicopathologic review of 233 cases in Lagos, Nigeria. *J Oral Maxillofac Surg* 2008; **66**: 1595–9.
12 Lam L, Logan RM, Luke C. Epidemiological analysis of tongue cancer in South Australia for the 24-year period, 1977–2001. *Aust Dent J* 2006; **51**: 16–22.
13 Thun MJ, Lally CA, Flannery JT, Calle EE, Flanders WD, Heath CW Jr. Cigarette smoking and changes in the histopathology of lung cancer. *J Natl Cancer Inst* 1997; **89**: 1580–86.
14 Travis WD, Travis LB, Devesa SS. Lung cancer. *Cancer* 1995; **75**: 191–202.
15 Grønbaek M, Becker U, Johansen D, Tønnesen H, Jensen G, Sørensen TI. Population based cohort study of the association between alcohol intake and cancer of the upper digestive tract. *BMJ* 1998; **317**: 844–7.
16 Macfarlane GJ, Macfarlane TV, Lowenfels AB. The influence of alcohol consumption on worldwide trends in mortality from upper aerodigestive tract cancers in men. *J Epidemiol Community Health* 1996; **50**: 636–9.

Cancer Research

Correlating Phosphatidylinositol 3-Kinase Inhibitor Efficacy with Signaling Pathway Status: *In silico* and Biological Evaluations

Shingo Dan[1], Mutsumi Okamura[1], Mariko Seki[1], Kanami Yamazaki[1], Hironobu Sugita[1], Michiyo Okui[2,3], Yumiko Mukai[1], Hiroyuki Nishimura[4], Reimi Asaka[2], Kimie Nomura[2], Yuichi Ishikawa[2], and Takao Yamori[1]

Abstract

The phosphatidylinositol 3-kinase (PI3K) pathway is frequently activated in human cancers, and several agents targeting this pathway including PI3K/Akt/mammalian target of rapamycin inhibitors have recently entered clinical trials. One question is whether the efficacy of a PI3K pathway inhibitor can be predicted based on the activation status of pathway members. In this study, we examined the mutation, expression, and phosphorylation status of PI3K and Ras pathway members in a panel of 39 pharmacologically well-characterized human cancer cell lines (JFCR39). Additionally, we evaluated the *in vitro* efficacy of 25 PI3K pathway inhibitors in addition to conventional anticancer drugs, combining these data to construct an integrated database of pathway activation status and drug efficacies (JFCR39-DB). *In silico* analysis of JFCR39-DB enabled us to evaluate correlations between the status of pathway members and the efficacy of PI3K inhibitors. For example, phospho-Akt and KRAS/BRAF mutations prominently correlated with the efficacy and the inefficacy of PI3K inhibitors, respectively, whereas *PIK3CA* mutation and PTEN loss did not. These correlations were confirmed in human tumor xenografts *in vivo*, consistent with their ability to serve as predictive biomarkers. Our findings show that JFCR39-DB is a useful tool to identify predictive biomarkers and to study the molecular pharmacology of the PI3K pathway in cancer. *Cancer Res; 70(12); 4982–94. ©2010 AACR.*

Introduction

Phosphatidylinositol 3-kinases (PI3K) are lipid kinases that phosphorylate phosphoinositide at position D3 of the inositol ring (1, 2). The catalytic subunit of class I PI3K is composed of four isoforms (p110α, p110β, p110δ, and p110γ, encoded by *PIK3CA, PIK3CB, PIK3CD*, and *PIK3CG*). Among these isoforms, *PIK3CA* is often activated in cancer by gain-of-function hotspot mutations (3, 4) and gene amplification (5, 6). On the other hand, phosphatase and tensin homologue deleted on chromosome 10 (PTEN) is a lipid phosphatase that dephosphorylates PIP3 at position D3 of the inositol ring to generate PIP2. *PTEN* has been shown to be a tumor suppressor gene and is often inactivated by deletion or mutation in cancer (7–9). Activation of PI3K and PTEN loss trigger sequential phosphorylation of the PI3K downstream signal cascade, including Akt and mammalian target of rapamycin (mTOR), and mediates a survival signal, as well as tumor proliferation (9). Therefore, the PI3K pathway is thought to be a promising therapeutic target.

LY294002 and wortmannin are first-generation PI3K inhibitors, but neither has progressed to clinical trials because of cytotoxicity to liver and skin (10, 11). We previously reported a selective PI3K inhibitor, ZSTK474, which has potent antitumor activity and low toxicity *in vivo* (12). Subsequently, several PI3K inhibitors have been developed, and some including NVP-BEZ235 and GDC-0941 have already entered clinical trials (13–15). In addition to PI3K inhibitors, antitumor compounds targeting Akt and mTOR have been developed (15–18).

To develop a molecular-targeted anticancer drug, it is highly desirable to develop predictive biomarkers for stratifying patients susceptible to the drug. In fact, mutations of *EGFR* and *KRAS* are used to predict the efficacy of gefitinib in lung cancer and that of cetuximab in colorectal cancer, respectively (19–22). Moreover, Engelman and colleagues recently showed that tumor growth triggered by KRAS mutant exhibited resistance to NVP-BEZ235 (23). On the other hand, dysregulation of *PIK3CA* and PTEN has been reported to be involved in resistance to EGFR-targeted therapies (24–26). As mentioned above, *PIK3CA* mutation and PTEN loss trigger

Authors' Affiliations: [1]Division of Molecular Pharmacology, Cancer Chemotherapy Center, and [2]Department of Pathology, Cancer Institute, Japanese Foundation for Cancer Research, Tokyo, Japan and [3]Department of Biomedical Engineering, Toin Human Science and Technology Center, and [4]Department of Biomedical Engineering, Toin University of Yokohama, Yokohama, Japan

Note: Supplementary data for this article are available at Cancer Research Online (http://cancerres.aacrjournals.org/).

Corresponding Author: Takao Yamori, Division of Molecular Pharmacology, Cancer Chemotherapy Center, Japanese Foundation for Cancer Research, 3-8-31 Ariake, Koto-ku, Tokyo 135-8550, Japan. Phone: 81-3-3520-0111 ext. 5432; Fax: 81-3570-0484; E-mail: yamori@jfcr.or.jp.

doi: 10.1158/0008-5472.CAN-09-4172

activation of the kinase cascade of the PI3K downstream pathway. However, it is not well understood whether the efficacy of PI3K pathway inhibitors could be predicted by these upstream abnormalities and downstream activities of the PI3K pathway.

We previously established a panel of 39 human cancer cell lines (JFCR39) derived from various organs (27–29). JFCR39, as well as NCI60 developed by National Cancer Institute, has been used as an *in vitro* tool to measure "fingerprints" of cytotoxic compounds. Fingerprints are defined as the patterns of differential drug efficacy across a panel of cell lines and have been found to reflect mechanisms of drug action (27–30). ZSTK474 is a compound that we identified as a new PI3K inhibitor based on the similarity with the fingerprint of LY294002 (12). In other words, each of the JFCR39 cell lines showed similar responses to ZSTK474 and LY294002, and the responses varied from cell line to cell line. This suggested that the status of biological pathways determining a cancer cell's response to PI3K inhibitors (which may include the PI3K pathway) is heterogeneous across these cell lines.

In the present study, taking advantage of JFCR39, we examined the mutation and/or expression of upstream regulators of the PI3K and Ras pathways, including four PI3K isoforms (*PIK3CA, PIK3CB, PIK3CD*, and *PIK3CG*), *PTEN*, the ERBB family receptor tyrosine kinases (RTKs), *KRAS* and *BRAF*, and the phosphorylation of downstream pathway members including Akt, TSC2, GSK-3, mTOR, S6K1, mitogen-activated protein kinase (MAPK)/extracellualr signal–regulated kinase (ERK) kinase (MEK)-1/2, and ERK1/2. Next, we examined the fingerprints of 25 compounds targeting the PI3K pathway as well as other conventional anticancer drugs. We then combined the PI3K and Ras pathway database and the drug database to develop an integrated database of pathway status and drug efficacies (JFCR39-DB). Using this database, we first evaluated the functional relationships among these pathway inhibitors and those among drugs by comparing their fingerprints. Second, we evaluated the correlation between PI3K pathway members and PI3K pathway inhibitors to identify candidate biomarkers for predicting their efficacy.

Materials and Methods

Cell lines and cell culture

A panel of 39 human cancer cell lines, termed JFCR39, were previously described (27, 28, 31). Cells were grown in RPMI 1640 (Wako Pure Chemical Industries Ltd.) supplemented with 1 μg/mL kanamycin and 5% (v/v) fetal bovine serum (Moregate Exports) and incubated at 37°C in a humidified atmosphere supplemented with 5% CO_2. Authentication of cell lines was done by short tandem repeat analysis using PowerPlex16 Systems (Promega; data not shown).

Amplification of genomic DNA fragments for sequencing

Extraction of genomic DNA was done using DNeasy blood and tissue kit (Qiagen) according to the manufacturer's instructions. Amplification of genomic DNA fragments was done using Pfu Ultra High-Fidelity DNA polymerase (Agilent Technologies), FastStart High Fidelity PCR System (Roche Applied Science), or AccuPrime Taq DNA Polymerase High Fidelity (Invitrogen). Polymerases and primer sequences used in each reaction are shown in Supplementary Table S1.

Nucleotide sequence analysis

Sequencing reactions were done using BigDye Terminator v3.1 and dGTP BigDye Terminator v3.0 (Applied Biosystems) according to the manufacturer's instructions. Primers were shown in Supplementary Table S1. Nucleotide sequences were analyzed using a 3130 Genetic Analyzer (Applied Biosystems) and sequence files were edited using 4 Peaks software (Mekentosj B.V.).

Detection of lipid kinase activities of PI3K p110α mutants

Determination of lipid kinase activities of PI3K p110α was described as previously (32). In brief, HEK293T cells were transfected with pFLAG-PIK3CA (with or without mutation) and pc-PIK3R1 using Lipofectamine 2000 (Invitrogen). After 48 hours of incubation, cells were harvested and the lysates were immunoprecipitated by using FLAG-Tagged Protein Immunoprecipitation Kit (Sigma-Aldrich). To detect kinase activity, we used the PI3K-HTRF assay kit (Millipore) and EnVision 2103 Mutilabel Reader (Perkin-Elmer).

Preparation of total cell extract

Cells were resuspended in lysis buffer [10 mmol/L Tris-HCl (pH 7.4)], 50 mmol/L NaCl, 0.5% w/v NP40, 0.1% w/v SDS, 50 mmol/L sodium fluoride, 30 mmol/L sodium pyrophosphate, 50 mmol/L sodium orthavanadate, 5 mmol/L EDTA, 0.1 trypsin inhibitor unit/mL aprotinin, and 1 mmol/L phenylmethylsulfonyl fluoride] and lysed by sonication in an ice bath. Concentrations of proteins in the extracts were determined using a protein assay kit (Pierce).

Immunoblot analysis

Equal amounts of protein were subjected to SDS-PAGE and the separated proteins were transferred onto an Immobilon FL polyvinylidene difluoride membrane (Millipore). The membrane was incubated with a primary antibody. The antibodies for PI3K p110α, Akt, phospho-Akt (T308, S473), phospho-GSK-3 (S9), phospho-TSC2 (T1462), phospho-mTOR (S2448), phospho-S6K1 (T389), phospho-MEK1 (S217/S221), and phospho-ERK1/2 (T202/Y204) were purchased from Cell Signaling Technologies. The antibodies for PI3K p110β, p110γ, and p110δ were purchased from Millipore. The antibody for PTEN was purchased from BD Biosciences Pharmingen. Bound antibody was quantitatively detected using an appropriate antimouse or rabbit immunoglobulin secondary antibody labeled with Alexa Fluor 680 (Invitrogen) and the Odyssey Infrared Imaging System (LI-COR). Data shown are median values of three independent experiments.

Table 1. Missense mutations of PI3K isoforms, *PTEN*, *KRAS*, and *BRAF* in JFCR39

ID	Origin	Cell line	*PIK3CA*	*PIK3CB*	*PIK3CD*	*PIK3CG*	*PTEN*	*KRAS*	*BRAF*
01	Lung ca.	NCI-H23				P538L		G12C	
02		NCI-H226				S442Y (SNP)			
03		NCI-H522							
04		NCI-H460	E545K (genomic)					Q61H	
05		A549						G12S	
06		DMS273				M259I	K128N		
07		DMS114							
11	Colorectal ca.	HCC2998	I391M (SNP)	R149Q R562Q		T857A R273H L466M	Y46C R130Q F341V	A146T	
12		KM-12					G129* K267fs(del.-1)*9		
13		HT-29	P449T			S442Y(SNP)			V600E
15		HCT-15	E545K D549N	R628Q	S174L			G13D	
16		HCT-116	H1047R		Ex.16 del.		G13D		
21	Gastric ca.	St-4				S442Y(SNP)	E291*	G12A	
22		MKN1	E545K						
23		MKN7			T456A (SNP)	A621S			
24		MKN28			T456A (SNP)	A621S			
25		MKN45							
26		MKN74			T456A (SNP)	A621S			
31	Breast ca.	HBC-4		E1051K		S442Y(SNP)			
32		BSY-1	H1047R				Ex.1-9 del.		
34		HBC-5							
35		MCF-7	E545K			S442Y(SNP)			
36		MDA-MB-231						G13D	G464V
41	Ovarian ca.	OVCAR-3							
42		OVCAR-4							
43		OVCAR-5						G12V	
44		OVCAR-8				N522S			
45		SK-OV-3	H1047R						
51	Brain ca.	U251					E242fs(ins.+2)*15		
52		SF-268							
53		SF-295			S312C		R233*		
54		SF-539					Ex.1-9 del.		
55		SNB-75							
56		SNB-78	L719F				T26fs(SD del.)		
61	Renal ca.	RXF-631L				S442Y(SNP)			
62		ACHN							
71	Melanoma	LOX-IMVI							V600E
91	Prostate ca.	DU-145		A686T		S442Y(SNP)			
92		PC-3			S312C	S442Y(SNP)	Ex.3-9 del.		
Total # (without SNP)			10 (9)	4	7 (4)	15 (7)	10	9	3

NOTE: Underline indicates a homozygous mutation.

Drugs

ZSTK474 was kindly provided by Zenyaku Kogyo Co. Ltd. LY294002, PI103, PI3Kα inhibitor IV, PI3Kγ inhibitor (AS605240), and Akt inhibitors II, III, IV, V (triciribine), VIII, IX, X, and XI were purchased from Calbiochem. TGX221 and perifosine were purchased from Cayman. GDC-0941 and IC87114 were obtained from Symansis. RAD001 and CCI779 were purchased from LC Laboratories. Wortmannin,

PX-866, NVP-BEZ235, and rapamycin were obtained from Kyowa Medex, Sigma, Selleck, and Wako Pure Chemical, respectively.

Determination of drug efficacy

Drug efficacy was assessed as changes in total cellular protein after 48 hours of drug treatment using a sulforhodamine B assay. Assays were done in duplicate and the GI_{50} was calculated as described previously (27, 33).

Animal experiments

Animal care and treatment were done in accordance with the guidelines of the animal use and care committee of the Japanese Foundation for Cancer Research and conformed to the NIH Guide for the Care and Use of Laboratory Animals. Female nude mice with BALB/c genetic backgrounds were purchased from Charles River Japan. Mice were maintained under specific pathogen-free conditions and provided with sterile food and water *ad libitum*. Human tumor xenografts were generated by s.c. inoculating nude mice with 3 mm × 3 mm × 3 mm tumor fragments of human cancer cells. When the tumors became 100 to 300 mm^3 in size, ZSTK474 was p.o. administered at 100, 200, and 400 mg/kg of body weight following the indicated schedule. The length (L) and width (W) of the subcutaneous tumor mass were measured by calipers in live mice, and the tumor volume (TV) was calculated as $TV = (L \times W^2)/2$. Percent treated/control [T/C (%)] was calculated as $(TV_{with\ drug}/TV_{control}) \times 100$. To assess toxicity, we measured the body weight of the tumor-bearing mice. Mice were finally sacrificed and tumors were excised and frozen in liquid N_2.

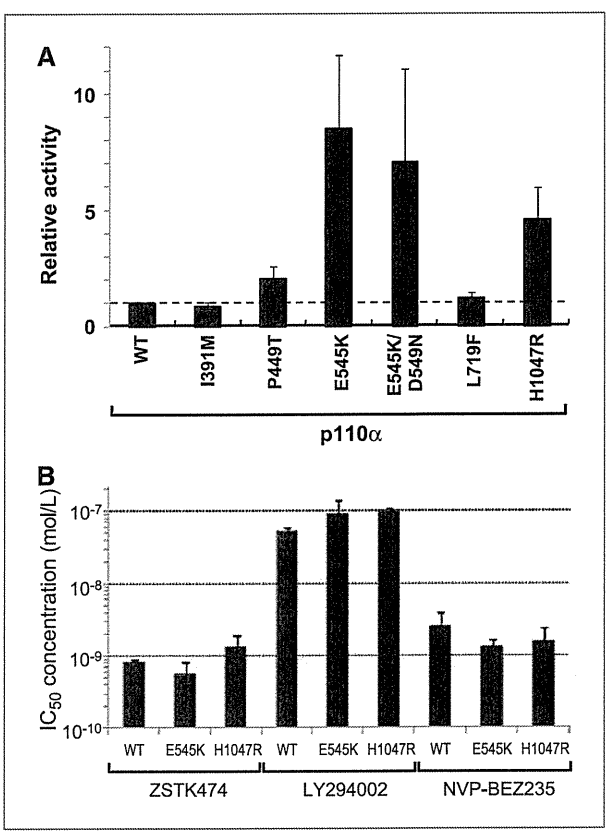

Figure 1. Relative kinase activities of p110α mutants and the inhibitory effect of PI3K inhibitors against hotspot mutants of p110α. A, recombinant FLAG-tagged PI3K p110α/p85α protein complex produced in 293T cells was immunoprecipitated, and the immunoprecipitates were used for the quantitative PI3K-HTRF assay (32). B, effect of three PI3K inhibitors (ZSTK474, LY294002, and NVP-BEZ235) on the enzymatic activity of two hotspot mutants (E545K and H1047R) p110α compared with the wild-type. No striking difference was observed in the IC_{50} concentrations of these inhibitors between wild-type and mutant p110α.

Results

Characterization of the mutation status of PIK3Cs, PTEN, KRAS, and BRAF in JFCR39 cell lines

We first examined the mutation status of PI3K isoforms in the JFCR39 cell lines (Table 1; Supplementary Table S2). Analysis of genomic sequences of *PIK3CA* on exon 9 and exon 20 revealed the hotspot mutations (E545K in four cell lines and H1047R in three cell lines). Analysis of the full coding sequence of cDNA revealed four additional missense mutations: I391M, P449T, D549N, and L719F. Evaluation of relative kinase activity of these mutants revealed that mutant P449T exhibited gain of function (>2-fold) compared with wild-type PI3Kα (Fig. 1A). The E545K mutation found in NCI-H460 genomic DNA was not detected in the cDNA, suggesting that the allele with the E545K mutation was hardly transcribed in NCI-H460 cells. Therefore, we concluded that seven cell lines [HCT-116, SK-OV3, BSY-1 (H1047R), MKN-1, MCF7 (E545K), HCT-15 (E545K/D549N), and HT-29 (P449T)] expressed a gain-of-function mutant of *PIK3CA*. With regard to two hotspot mutants (E545K and H1047R), we examined the effect of three representative PI3K inhibitors on their enzymatic activity and found no striking difference in their efficacies compared with wild-type p110α (Fig. 1B).

In addition to *PIK3CA*, we examined the genomic sequences of all coding exons of *PIK3CB, PIK3CD*, and *PIK3CG* genes and found five missense mutations in *PIK3CB*, three in *PIK3CD*, and eight in *PIK3CG* (Table 1; Supplementary Table S2). Most of these mutations were not registered in the dbSNP database established by The National Center for Biotechnology Information. Therefore, this study is the first report showing that cancer cells harbor missense mutations in *PIK3CB, PIK3CG*, and *PIK3CD* as well as in *PIK3CA*.

Next, we proceeded to examine the genomic sequences of the *PTEN* gene and found that the *PTEN* gene was deleted in three cell lines (BSY-1, SF539, and PC-3), and seven had missense or frameshift mutations.

We examined the genomic sequences of exon 1 (including G12 and G13) and exon 2 (Q61) of *KRAS* and exon 15 (V600) and exon 11 (G464, G466, and G468) of *BRAF* (Table 1). Eight of 39 cell lines had a hotspot mutation in the G12, G13, or Q61 residue. On the other hand, the *BRAF* mutation was observed in three cell lines including LOX-IMV1.

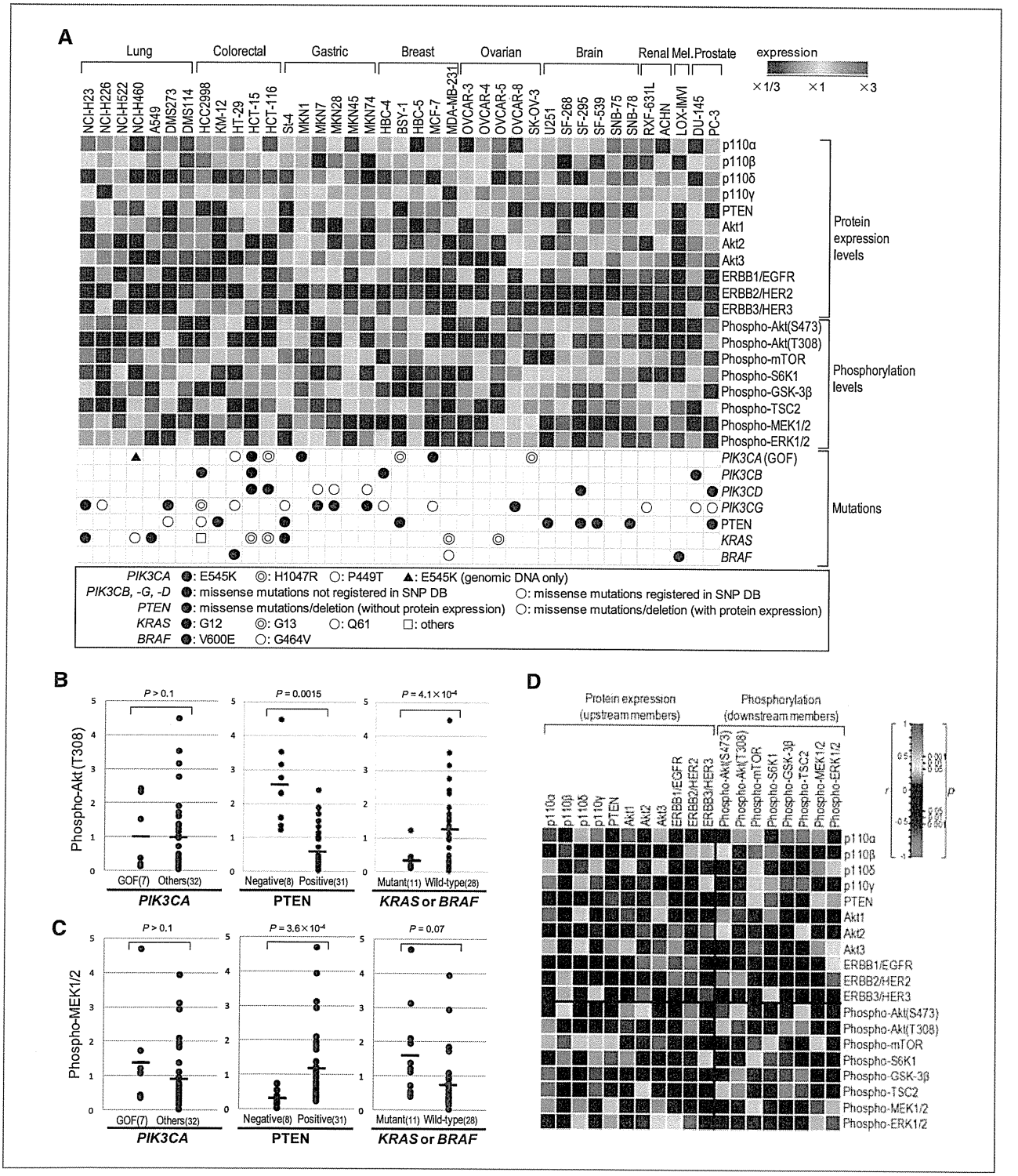

Figure 2. Mutation, protein expression, and phosphorylation status of PI3K and Ras pathway members and the correlation among them. A, the protein expression of upstream members and the phosphorylation of downstream members in each of the JFCR39 cell lines were determined by immunoblot analysis and normalized so that their average across the JFCR39 cell lines was 1 (yellow). A red point and a blue point represent high and low expression by 3-fold, respectively. Mutation data are from Table 1. B and C, differences in expression levels of phospho-Akt (T308) (B) and phospho-MEK1/2 (C) between cell lines with or without *PIK3CA* gain-of-function mutation (GOF), PTEN expression, and *KRAS/BRAF* mutation. Student's *t* tests were used to examine significance of differential expression. D, a heat map representing the similarities among the fingerprints of PI3K pathway members. Red to yellow: significant positive correlation ($P < 0.05$); yellow to black, black to blue: no significant correlation ($P > 0.05$), blue to sky blue: significant negative correlation ($P < 0.05$).

Expression of PI3K isoforms, PTEN, Akt isoforms, and ERBB-family RTKs

We next examined the protein expression of upstream members of the PI3K pathway that would affect downstream activity, including PI3K isoforms (p110α/β/γ/δ), PTEN, Akt isoforms (Akt1/2/3), and ERBB-family RTKs (EGFR/ERBB2/ERBB3; Fig. 2A; Supplementary Data). As expected, p110α and p110β were widely expressed, whereas p110γ and p110δ, which were thought to be expressed preferentially in leukocytes, were unexpectedly expressed in most JFCR39 cell lines derived from solid tumors. PTEN expression was undetectable in all of three cell lines with the deletion and in five of seven cell lines with a mutation, whereas all of 29 cell lines lacking a mutation or deletion expressed a certain amount of PTEN protein (Supplementary Fig. S1). Some of the cell lines exhibited overexpression of Akt isoforms; SF268 and MCF-7 highly expressed Akt1, whereas OVCAR3 and HBC5 highly expressed Akt2. EGFR was expressed in a wide variety of cell lines, but in some cell lines including NCI-H522 and MCF-7, EGFR expression was absent or present at an extremely low level. ERBB3 was highly expressed in a wide variety of cell lines derived from ovarian, gastric, breast, and colorectal cancer cell lines, but not in most brain cancer cell lines. On the other hand, ERBB2 was highly expressed in two cell lines (SK-OV-3 and HBC5).

Activation status of downstream members of the PI3K pathway

We examined the phosphorylation levels of PI3K downstream effectors including Akt (phosphorylated on T308 and S473), mTOR (S2448), S6K1 (T389), GSK-3β (S9), and TSC2 (T1462; Fig. 2A). We also examined Ras downstream effectors, phosphorylated MEK1/2 (S217/S221) and ERK1/2 (T202/Y204). Interestingly, the expression pattern of phosphorylated Akt (T308) was highly correlated with phosphorylated TSC2 ($r = 0.70$) and GSK-3β ($r = 0.60$), but not with phosphorylated mTOR and S6K1 (Fig. 2A; Supplementary Fig. S2). On the other hand, expression levels of phosphorylated Akt (T308) had a significant negative correlation with phosphorylated ERK1/2 ($r = 0.39$).

Correlation between upstream abnormalities and phosphorylation of downstream effectors in the PI3K pathway

Correlation analysis between upstream abnormalities and downstream activities revealed some interesting results (Fig. 2B and C; Supplementary Table S3). For example, phosphorylation levels of Akt (T308) ($P = 0.0015$) and TSC2 ($P = 0.011$) were significantly higher and those of MEK1/2 ($P = 3.6 \times 10^{-4}$) and ERK1/2 ($P = 2.7 \times 10^{-5}$) were significantly lower in eight PTEN-negative cell lines than those in 31 PTEN-expressing cell lines. This suggested that PTEN loss conferred activation of PI3K downstream factors and inactivation of the MAPK pathway. In contrast, phosphorylation levels of Akt (T308) ($P = 4.1 \times 10^{-4}$) and TSC2 ($P = 0.0021$) were significantly lower in cell lines having a mutation in either the *KRAS* or the *BRAF* gene, suggesting inactivation of the PI3K/Akt pathway in these cell lines. However, mutation of *PIK3CA* did not have significant associations with downstream activation, including phosphorylation levels of Akt and MEK.

Determination of efficacy patterns of 25 PI3K pathway inhibitors across JFCR39 cell lines, or fingerprints, and evaluation of their modes of action from their fingerprints

We next examined the efficacy of 25 PI3K pathway inhibitors (Table 2) in each of the JFCR39 cell lines. Then, we compared the fingerprints of PI3K inhibitors with those of other conventional anticancer drugs by cluster analysis (Fig. 3A; Supplementary Fig. S3A). Interestingly, 10 of 11 PI3K inhibitors were tightly clustered and the cluster also included Akt inhibitor VIII (AKTi-1/2) and rapamycins, suggesting similarity in the mechanisms of action across these compounds. Moreover, their fingerprints were clearly different from those of the remainder of the 10 Akt inhibitors, all of three MEK inhibitors, and other conventional anticancer drugs. Furthermore, comparison of the fingerprints of 15 PI3K pathway inhibitors in the cluster revealed that some pairs, including ZSTK474/GDC-0941 ($r = 0.86$), wortmannin/PX-866 ($r = 0.81$), and PI103/PI3Kα inhibitor IV ($r = 0.80$), exhibited extremely high correlations, suggesting a close similarity in the molecular mechanisms of action between each pair of compounds (Supplementary Fig. S3B–D).

Construction of an integrated database and correlations between the status of pathway members and the efficacy of PI3K inhibitors

We have thus far studied the drug efficacy data and the signal pathway data with regard to JFCR39 cell lines. We then combined these data to develop an integrated database (JFCR39-DB). Using JFCR39-DB, we studied the relationship between the activation status of the PI3K pathway and the efficacy of PI3K pathway inhibitors. First, we examined the correlation between the mutation status of upstream members and drug efficacy. The Student *t* test revealed no significant differences in the efficacies of all of 25 PI3K pathway inhibitors examined, in seven cell lines expressing a gain-of-function mutant of PI3Kα, and in the remainder of the 32 cell lines (Fig. 3B; Supplementary Table S4). As mentioned before, we examined the effect of three representative PI3K inhibitors on the enzymatic activity of two hotspot mutants of PI3Kα and found no striking difference in their efficacies compared with wild-type p110α (Fig. 1B). These results suggest that cancer cells expressing mutant PI3Kα are susceptible to PI3K inhibitors to a similar extent as those expressing wild-type PI3Kα. Moreover, PTEN status did not correlate with the efficacy of PI3K pathway inhibitors. In addition, the mutation status of other PI3K isoforms did not exhibit striking correlations either. On the other hand, cell lines having a mutation in either *KRAS* or *BRAF* exhibited resistance to several PI3K pathway inhibitors including ZSTK474 (Fig. 3B; Supplementary Table S4). The present results suggest that *KRAS/BRAF*

Table 2. The 25 PI3K pathway inhibitors used in this study and their profiles and structures (15–18)

PI3K inhibitors

ZSTK474 (4.8×10^{-7} mol/L) Selective PI3K inhibitor Preclinical	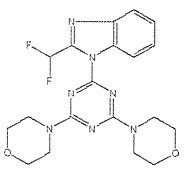	Wortmannin (9.7×10^{-6} mol/L) PI3K/mTOR/MLCK inhibitor Preclinical	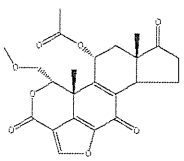
LY294002 (8.1×10^{-6} mol/L) PI3K/mTOR/CK2 inhibitor Preclinical	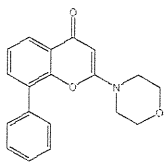		
PI103 (1.8×10^{-7} mol/L) PI3K/mTOR inhibitor Preclinical	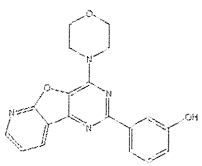	PX866 (1.4×10^{-6} mol/L) PI3Kα/δ/γ inhibitor; derivative of wortmannin Phase I	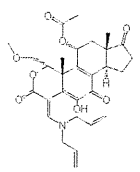
NVP-BEZ235 (8.6×10^{-9} mol/L) PI3K/mTOR inhibitor Phase I/II	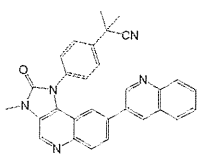		
GDC-0941 (5.0×10^{-7} mol/L) Selective PI3K inhibitor Phase I	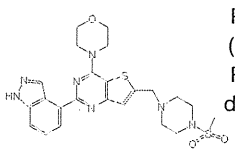	PI3Kα inhibitor IV (1.0×10^{-6} mol/L) PI3Kα/β inhibitor; derivative of PI103 Preclinical	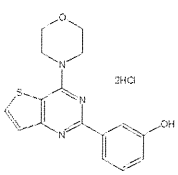
TGX221 (1.0×10^{-5} mol/L) Selective PI3Kβ inhibitor Preclinical	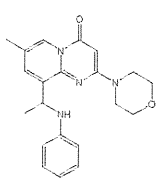		
IC87114 (CAL-101; 8.3×10^{-5} mol/L) Selective PI3Kδ inhibitor Phase I	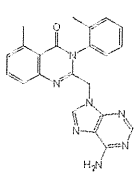	AS605240 (PI3Kγ inhibitor; 9.5×10^{-6} mol/L) Selective PI3Kγ inhibitor Preclinical	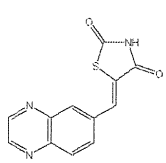

Akt inhibitors

Deguelin (7.6×10^{-6} mol/L) Selective Akt inhibitor; derivative of rotenone Preclinical	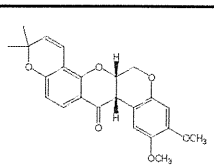	Perifosine (9.1×10^{-6} mol/L) Lipid-based PI analogue Phase II	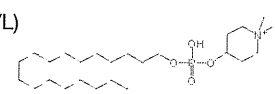
Akt inhibitor (1.3×10^{-5} mol/L) Lipid-based PI analogue Preclinical	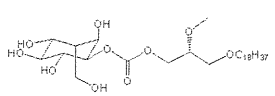		
Akt inhibitor II (8.6×10^{-6} mol/L) Lipid-based PI analogue Preclinical	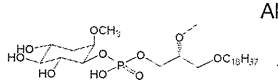	Akt inhibitor III (1.9×10^{-5} mol/L) Lipid-based PI analogue Preclinical	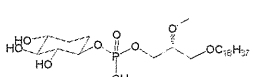
Akt inhibitor IV (2.8×10^{-7} mol/L) Preclinical	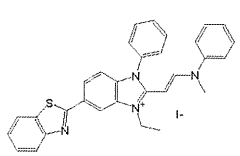		
Akt inhibitor V (triciribine/ VQD-002; 2.2×10^{-5} mol/L) Tricyclic nucleotide Phase I/II (as triciribine phosphate)	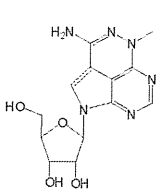	Akt inhibitor VIII (AKTi-1/2; 8.6×10^{-6} mol/L) Allosteric Akt1/2 inhibitor Preclinical	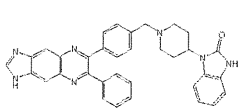
Akt inhibitor IX (8.0×10^{-7} mol/L) Preclinical	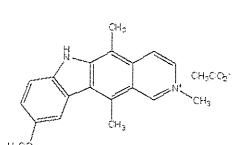		

(*Continued on the following page*)

Table 2. The 25 PI3K pathway inhibitors used in this study and their profiles and structures (15–18) (Cont'd)

Akt inhibitors			
Akt inhibitor X (3.6×10^{-6} mol/L) Preclinical	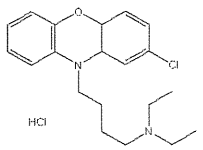	Akt inhibitor XI (1.1×10^{-5} mol/L) Preclinical	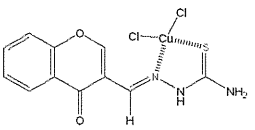
mTOR inhibitors			
Rapamycin (1.7×10^{-7} mol/L) Allosteric inhibitor of mTORC1 In clinical use	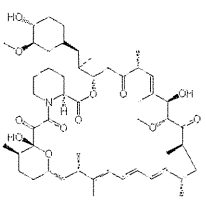	Everolimus (RAD001; 3.6×10^{-8} mol/L) Rapalogue In clinical use	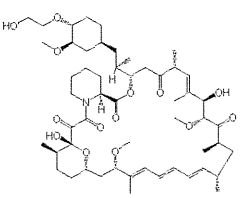
Temsirolimus (CCI779; 2.0×10^{-7} mol/L) Rapalogue In clinical use	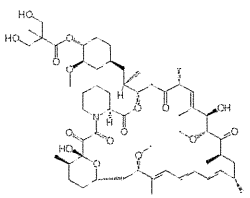		

NOTE: Numbers in parentheses are mean GI_{50} values across the JFCR39 cell lines.

mutation would be a biomarker for resistance to these PI3K pathway inhibitors.

Correlation of the efficacy of PI3K pathway inhibitors with protein expression levels of PI3K isoforms, Akt isoforms, and ERBB-family RTKs

We next correlated the expression levels of the above proteins with the efficacy of PI3K pathway inhibitors (Fig. 3A). As a result, we found that expression of p110α had a slight positive correlation with four PI3K inhibitors including IC87114 and LY294002. As for p110β, we found that its high expression correlated with the efficacy of several Akt inhibitors including perifosine. As for Akt isoforms, we found that high expression of Akt2 was associated with the efficacy of five PI3K pathway inhibitors including TGX-221 and LY294002. Correlation analysis between the expression levels of ERBB-family RTKs and the efficacy of PI3K inhibitors revealed no significant correlations with PI3K pathway inhibitors. However, high expression of EGFR correlated with resistance to other classes of anticancer drugs such as navelbine ($r = -0.49$) and mitoxantrone ($r = -0.43$), suggesting that EGFR would confer resistance to these drugs in cancer cells.

Correlation of the efficacy of PI3K pathway inhibitors with phosphorylation levels of the PI3K/Akt and Ras/MAPK pathways

Lastly, we correlated the phosphorylation levels of downstream members of the PI3K pathway with drug efficacy (Fig. 3A). Of note, expression of Akt phosphorylated at S473 had significant correlations with 11 of 25 inhibitors including ZSTK474 ($r = 0.44$; Fig. 3C) and wortmannin ($r = 0.52$). In addition, phosphorylated TSC2 correlated with 7 of 25 inhibitors, including Akt inhibitor IX ($r = 0.41$) and CCI779 ($r = 0.40$). This result suggests that expression levels of Akt phosphorylated at S473 and phosphorylated TSC2 would be predictive markers for these PI3K pathway inhibitors.

Phosphorylated Akt levels and KRAS/BRAF mutation correlated with the *in vivo* efficacy of ZSTK474

We have thus far studied correlations between the status of pathway members and the efficacy of PI3K inhibitors *in vitro*. The most prominent associations were that phosphorylated Akt correlated with the efficacy whereas *KRAS/BRAF* mutation correlated with the inefficacy of PI3K inhibitors including ZSTK474. To test these correlations *in vivo*, we inoculated 24 transplantable cell lines of JFCR39 and examined the antitumor effect of ZSTK474 (Supplementary Fig. S4). We first confirmed that the *in vitro* efficacy pattern across the 24 cell lines significantly correlated with the *in vivo* efficacy pattern (200 mg/kg; $P = 0.02$), suggesting that the *in vivo* efficacy of ZSTK474 reflected its *in vitro* efficacy (Supplementary Fig. S5). Based on these data, we examined the involvement of phosphorylated Akt and *KRAS/BRAF* mutation in the efficacy of ZSTK474 *in vivo* (Fig. 4). The Student *t* test revealed that cell lines having a hotspot mutation in either *KRAS* (G12, G13, and Q61) or *BRAF* (V600) exhibited inefficacy of ZSTK474 ($P = 0.04$; Fig. 4B). Cell lines with PTEN loss such as PC-3 and BSY-1 exhibited susceptibility to ZSTK474, but the difference was not statistically significant across the 24 cell lines. On the other hand, expression levels of phosphorylated Akt in the xenografted tumors significantly correlated with susceptibility to ZSTK474 (Fig. 4C). These results suggest that phosphorylated Akt and *KRAS/BRAF* hotspot mutation could be used as a biomarker for predicting the efficacy of PI3K inhibitors in the clinic.

Discussion

In this study, taking advantage of the JFCR39 cell line panel, we examined the drug efficacy of PI3K pathway inhibitors as well as the status of PI3K and Ras pathway members, and combined them to develop an integrated database. This

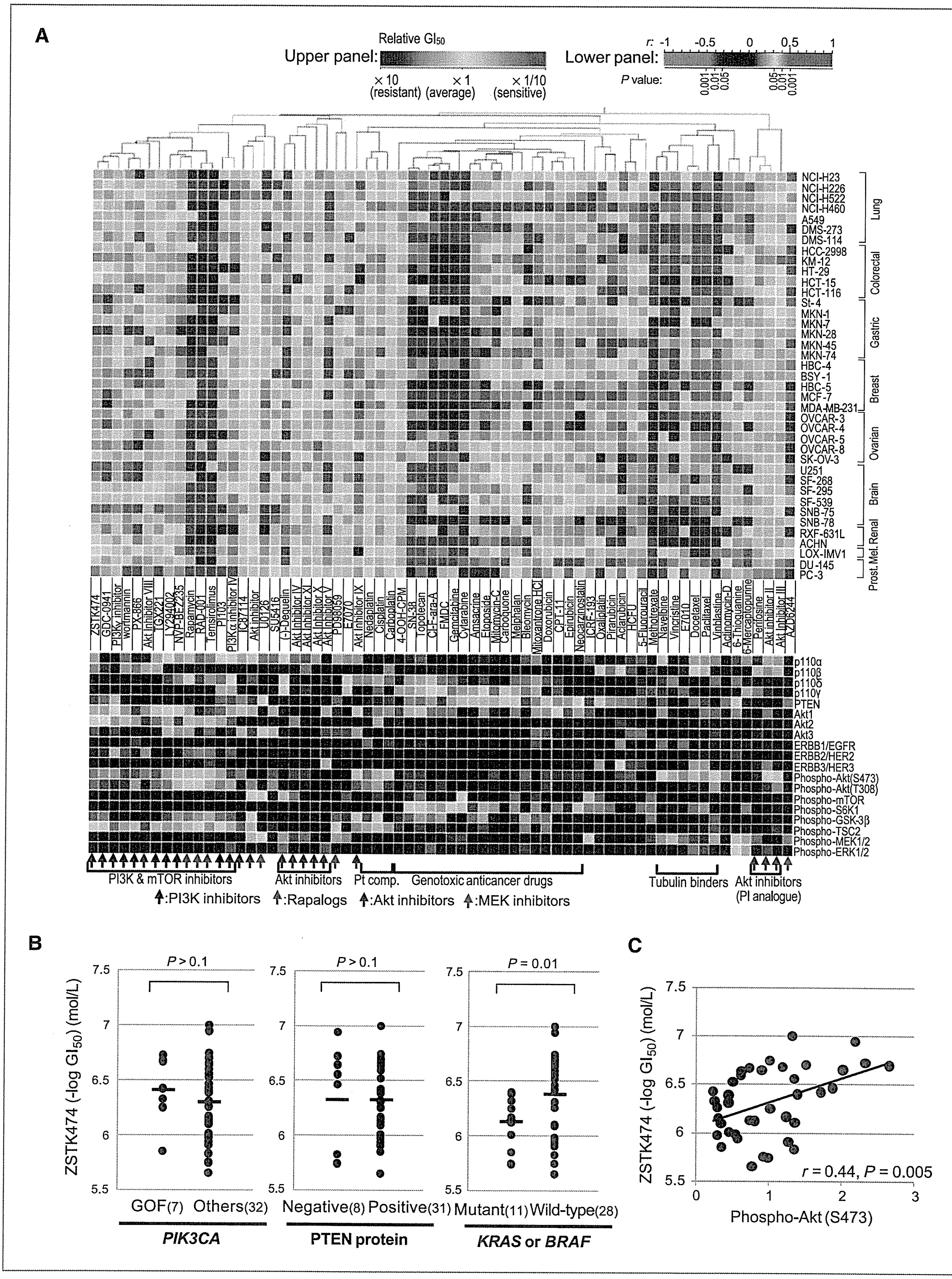
A
Relative GI50
Upper panel:
×10 (resistant)
×1 (average)
×1/10 (sensitive)
Lower panel:
r: -1 -0.5 0 0.5 1
P value: 0.001 0.01 0.05 0.05 0.01 0.001
NCI-H23
NCI-H226
NCI-H522
NCI-H460
A549
DMS-273
DMS-114
Lung
HCC-2998
KM-12
HT-29
HCT-15
HCT-116
Colorectal
St-4
MKN-1
MKN-7
MKN-28
MKN-45
MKN-74
Gastric
HBC-4
BSY-1
HBC-5
MCF-7
MDA-MB-231
Breast
OVCAR-3
OVCAR-4
OVCAR-5
OVCAR-8
SK-OV-3
Ovarian
U251
SF-268
SF-295
SF-539
SNB-75
SNB-78
Brain
RXF-631L
ACHN
Renal
LOX-IMVI
Mel.
DU-145
PC-3
Prost.
ZSTK474
GDC-0941
PI3Kγ inhibitor
wortmannin
PX-866
Akt inhibitor VIII
LY294002
NVP-BEZ235
Rapamycin
RAD-001
Temsirolimus
PI103
PI3Kα inhibitor IV
TC87114
Akt inhibitor
U0126
SU5416
(-)-Deguelin
Akt inhibitor IV
Akt inhibitor XI
Akt inhibitor X
Akt inhibitor V
PD98059
E7070
Akt inhibitor IX
Nedaplatin
Cisplatin
Carboplatin
4-OOH-CPM
SN-38
Topotecan
Cl-F-ara-A
FMDC
Gemcitabine
Cytarabine
Amsacrine
Etoposide
Mitomycin-C
Carboquone
Melphalan
Bleomycin
Mitoxantrone HCl
Doxorubicin
CPT-11
Epirubicin
Neocarzinostatin
ICRF-193
Oxaliplatin
Pirarubicin
Aclarubicin
HCFU
5-Fluorouracil
Methotrexate
Navelbine
Vincristine
E7010
Docetaxel
Paclitaxel
Vinblastine
Actinomycin-D
6-Thioguanine
6-Mercaptopurine
Perifosine
Akt inhibitor II
Akt inhibitor III
AZD6244
p110α
p110β
p110δ
p110γ
PTEN
Akt1
Akt2
Akt3
ERBB1/EGFR
ERBB2/HER2
ERBB3/HER3
Phospho-Akt(S473)
Phospho-Akt(T308)
Phospho-mTOR
Phospho-S6K1
Phospho-GSK-3β
Phospho-TSC2
Phospho-MEK1/2
Phospho-ERK1/2
PI3K & mTOR inhibitors
Akt inhibitors
Pt comp.
Genotoxic anticancer drugs
Tubulin binders
Akt inhibitors (PI analogue)
:PI3K inhibitors
:Rapalogs
:Akt inhibitors
:MEK inhibitors
B
ZSTK474 (-log GI50) (mol/L)
P > 0.1
P > 0.1
P = 0.01
GOF(7)
Others(32)
PIK3CA
Negative(8)
Positive(31)
PTEN protein
Mutant(11)
Wild-type(28)
KRAS or BRAF
C
r = 0.44, P = 0.005
Phospho-Akt (S473)

database, designated as JFCR39-DB, enabled us to evaluate correlations between the status of pathway members and drug efficacy, as well as correlations among pathway members and among inhibitors *in silico*. First, comparison of the status of pathway members revealed that PTEN loss significantly correlated with upregulated phosphorylation levels of PI3K downstream members and with downregulated phosphorylation levels of Ras downstream members, whereas *KRAS/BRAF* mutation exhibited an opposite tendency. Second, comparison of drug efficacies revealed that most PI3K inhibitors and rapamycins were tightly clustered and were clearly different from other classes of anticancer compounds, suggesting a similarity in the mechanisms of action across these compounds in the cluster. Third, correlation analysis between the status of pathway members and drug efficacy revealed that phosphorylated Akt and *KRAS/BRAF* hotspot mutation correlated with the efficacy and the inefficacy of PI3K inhibitors, respectively. These correlations were confirmed in xenografted human tumors *in vivo*, suggesting that they could serve as predictive biomarkers for PI3K inhibitors.

Correlation analysis among the pathway members revealed that PTEN loss significantly correlated with the phosphorylation levels of Akt, GSK-3β, and TSC2, but *PIK3CA* mutation did not exhibit such correlations, suggesting that PTEN loss was directly connected with activation of these downstream pathway members. Similar results were recently shown by Vasudevan and colleagues using NCI60 cell lines (34) and by Stemke-Hale and colleagues using clinical specimens and cell lines of human breast cancer (35), indicating the significance of PTEN loss in the activation of the PI3K pathway. Furthermore, we showed that PTEN loss was not accompanied by activation of mTOR and S6K1, suggesting the existence of upstream molecule(s) other than Akt that may regulate the activation of mTOR and S6K1. Indeed, mTOR is regulated by energy stress via AMPK and by hypoxia via HIF1α, as well as by growth factor stimulation via PI3K/Akt (13). Interestingly, PTEN loss was strongly associated with inactivation of MAPK pathway components such as MEK1/2 and ERK1/2. Previously, Zimmermann and Moelling reported that phosphorylation of Raf by Akt inhibited activation of the Ras/Raf/MAPK pathway (36), which supports our observation. On the other hand, mutation in either *KRAS* or *BRAF* was strongly correlated with inactivation of PI3K/Akt, rather than activation of the MAPK pathway. This result strongly suggests that gain-of-function mutations of *KRAS* and *BRAF* confer inactivation on Akt and its downstream pathway.

In this study, we performed a mutation analysis of all coding exons of *PIK3CB, PIK3CD*, and *PIK3CG* isoforms, which are thought to be rarely mutated in cancer (3). Unexpectedly, we found missense mutations in each isoform that were not registered in the SNP database. Although we could not determine whether they were cancer-specific somatic mutations or derived from germline mutations that have not yet been registered in the SNP database, this is the first report showing that cancer cells harbor missense mutations in these PI3K isoforms. The kinase activities of these mutants compared with their wild-type analogues are under investigation. Cancer cells having these mutations did not exhibit hyperphosphorylation of Akt and its downstream factors, suggesting that they did not activate the canonical PI3K pathway via Akt.

We previously showed that the fingerprints of antitumor compounds across the JFCR39 cell panel can allow evaluation of similarities in the cellular mechanism of action by which drugs exert their antitumor activity (28, 29). Comparison of drug fingerprints revealed that most PI3K inhibitors and rapamycins were tightly clustered and their fingerprints were clearly different from those of other classes of anticancer compounds, suggesting that they act by similar mechanisms, probably by blocking the PI3K/mTOR pathway. Moreover, a fine comparison of the fingerprints of these PI3K pathway inhibitors revealed that ZSTK474 and GDC-0941, both of which are specific class I PI3K inhibitors that do not inhibit other PI3K-related protein kinases including mTOR (15, 37–39), show similar fingerprints ($r = 0.86$). On the other hand, NVP-BEZ235, which is a more potent inhibitor of mTOR than of PI3K (40), exhibited high correlations with the mTOR inhibitor rapamycin ($r = 0.78$), and the correlation was much higher than those with ZSTK474 ($r = 0.67$) and GDC-0941 ($r = 0.46$). Thus, these results suggest that comparison of fingerprints may accurately distinguish the cellular target(s) that determine(s) the susceptibility of cancer cells to these drugs.

Using the integrated PI3K database, we correlated the status of these pathway members with the efficacy of PI3K inhibitors. We first found that either gain-of-function mutation of *PIK3CA* or PTEN loss did not exhibit significant correlation with the efficacy of PI3K inhibitors. Brachmann and colleagues recently reported that NVP-BEZ235 selectively induced apoptosis in *PIK3CA*-mutant breast cancer cells (41). However, in the present study, *PIK3CA*-mutant cell lines did not exhibit hypersensitivity but were susceptible to PI3K inhibitors to a similar extent as those with wild-type *PIK3CA*. Indeed, similar results were obtained in *in vivo* experiments using 24

Figure 3. Fingerprints of 67 compounds including 25 PI3K pathway inhibitors and other conventional anticancer agents and their correlations with the activation status of PI3K pathway members. A, top, the GI_{50} in each cell line was determined and log transformed. The compounds were clustered on the basis of their correlations with other compounds (average-linkage clustered with Pearson correlation metric). Cluster analysis was done by using GeneSpring GX (Agilent Technologies). A yellow point represents the average |log GI_{50}| for each compound across JFCR39. A red point and a blue point represent sensitivity and resistance by 10-fold, respectively. Bottom, a heat map of correlation between the fingerprints of 67 anticancer compounds and those of PI3K pathway members. A red point (high positive Pearson correlation coefficient, $P < 0.001$) indicates that the compound tends to be more effective against cell lines that express more of the protein; a blue point (high negative correlation, $P < 0.001$) indicates the opposite tendency. B, difference in the efficacy of ZSTK474 between cell lines with and without *PIK3CA* gain-of-function mutation, loss of PTEN expression, and *KRAS/BRAF* mutation. C, scatter plots of JFCR39 cell lines showing a significant correlation between phospho-Akt (S473) and the efficacy of ZSTK474.

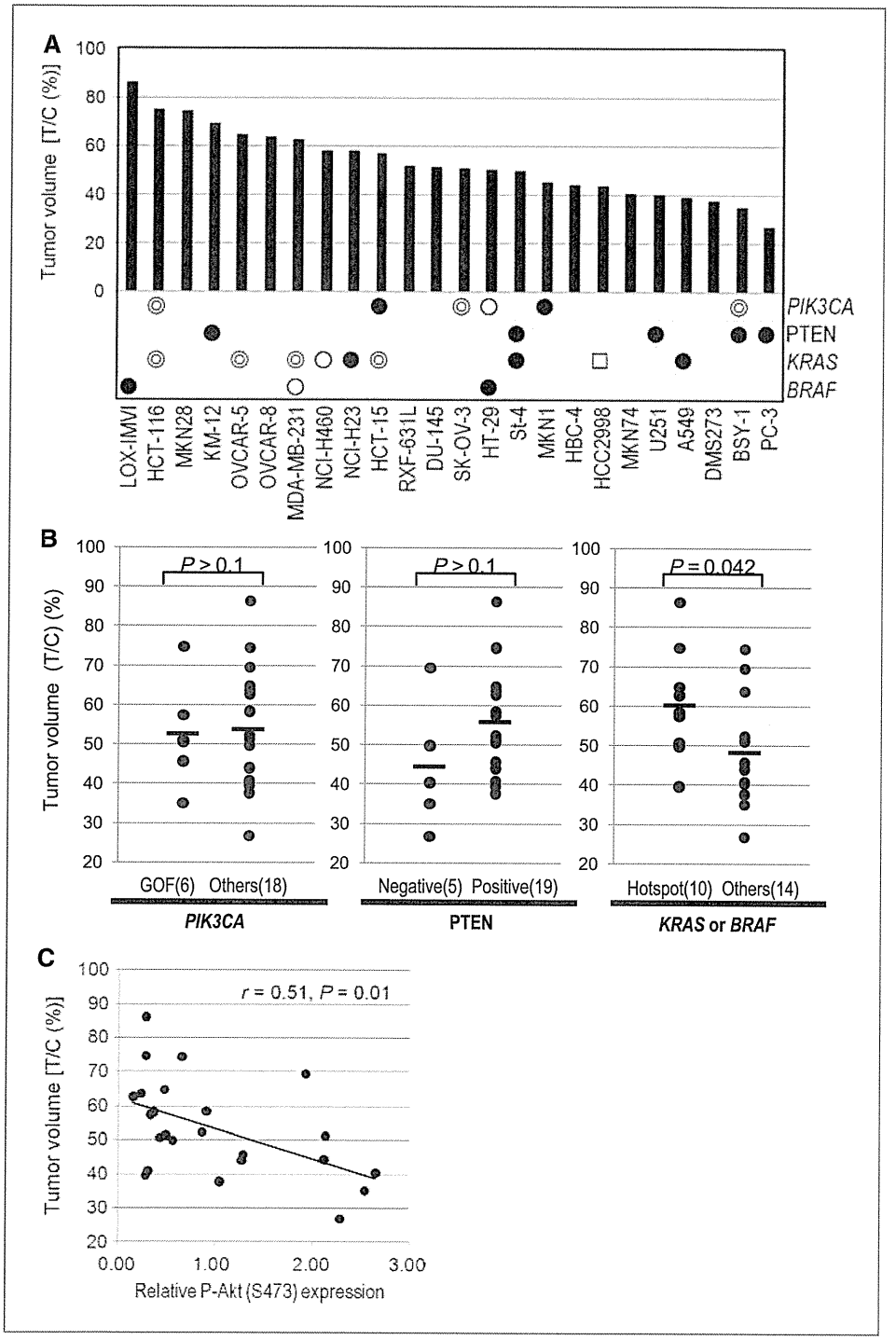

Figure 4. *In vivo* efficacy of ZSTK474 toward human tumors xenografted in nude mice and the activation status of PI3K pathway members. A, 24 transplantable cell lines of JFCR39 were inoculated in nude mice and the *in vivo* efficacy of ZSTK474 (200 mg/kg) was examined (T/C%). The mutation status of *PIK3CA* (closed circle: E545K, double circle: H1047R, open circle: P449T), *PTEN* (closed circle: mutation or deletion without protein expression), *KRAS* (closed circle: G12, double circle: G13, open circle: Q61, open square: A146), and *BRAF* (closed circle: V600E, open circle: G464V) were indicated. B, difference in the *in vivo* efficacy of ZSTK474 between cell lines with and without *PIK3CA* gain-of-function mutation, loss of PTEN expression, and *KRAS/BRAF* hotspot mutation. C, scatter plots of 24 cancer cell lines showing significant correlations between phospho-Akt (S473) expressed in tumor sample and the *in vivo* efficacy of ZSTK474.

transplantable human cancer cell lines xenografted in nude mice (Fig. 4B). We further showed that PI3K inhibitors including ZSTK474 and NVP-BEZ235 inhibit the enzymatic activity of gain-of-function mutant of p110α to an extent comparable to the wild-type (Fig. 1B). These results suggest that such PI3K inhibitors can be used for these cancers. On the other hand, cell lines with mutation in either *KRAS* or *BRAF* exhibited resistance to five PI3K inhibitors including ZSTK474. In *in vivo* studies, we showed that *KRAS/BRAF* mutation exhibited a significant correlation with efficacy of ZSTK474 using 24 xenografted tumors. Similar results were recently reported by Ihle and colleagues by using PX-866 and 13 human tumor xenografts (42) and by Engelman and colleagues using NVP-BEZ235 and a mouse tumor model ectopically expressing a KRAS mutant (23), suggesting the significance of *KRAS/BRAF* mutation in the inefficacy of these PI3K inhibitors.

Of the PI3K pathway downstream members examined in this study, it should be noted that Akt phosphorylated at S473 had significant correlations with 6 of 11 PI3K inhibitors including ZSTK474. Moreover, the correlation between phosphorylated Akt levels and the efficacy of ZSTK474 was confirmed in *in vivo* experiments using 24 human cancer xenografts. This result indicated that the expression level of Akt phosphorylated at S473 could be a candidate biomarker for predicting the efficacy of PI3K inhibitors. The reason why Akt phosphorylated at S473, but not T308, exhibited this correlation is unknown. Phosphorylation of the S473 residue of Akt is known to be catalyzed by the TORC2 complex (whose components include mTOR and rictor) and is required, in addition to T308, for full activation of Akt (43). It is intriguing that the fully activated form of Akt correlated with the efficacy of PI3K inhibitors.

In summary, we constructed an integrated database of PI3K and Ras pathway members and the efficacy of PI3K pathway inhibitors in JFCR39 (JFCR39-DB). *In silico* correlation analysis using JFCR39-DB enabled us to extract two candidates, phospho-Akt and *KRAS/BRAF* mutation, as predictive biomarkers for efficacy of PI3K inhibitors from various pathway members examined. Moreover, we confirmed these correlations by *in vivo* studies using 24 xenografted tumors. The utility of these candidate biomarkers should be validated through clinical studies in future. In addition, JFCR39-DB enabled us to study functional relationships among pathway members and those among drugs. Therefore, JFCR39-DB described here is a useful tool to identify predictive biomarkers, as well as to study the molecular pharmacology of the PI3K pathway in cancer.

Disclosure of Potential Conflicts of Interest

T. Yamori: commercial research grant, Zenyaku Kogyo Co., Ltd. The other authors disclosed no potential conflicts of interest.

Acknowledgments

We thank Yumiko Nishimura and Yoshimi Ohashi for their technical assistance and Zenyaku Kogyo Co. Ltd. for providing us with ZSTK474.

Grant Support

National Institute of Biomedical Innovation, Japan, grant 5-13 (T. Yamori); Grants-in-Aid of the Priority Area "Cancer" from the Ministry of Education, Culture, Sports, Science, and Technology of Japan, nos. 18015049 and 20015048 (T. Yamori); Grants-in-Aid for Scientific Research (B), no. 17390032, and (A), no. 22240092, from the Japan Society for the Promotion of Science (T. Yamori); the Kobayashi Institute for Innovative Cancer Chemotherapy (T. Yamori); and Grants-in-Aid for Young Scientists (B) from the Japan Society for the Promotion of Science, nos. 20790087and 22700929 (S. Dan).

The costs of publication of this article were defrayed in part by the payment of page charges. This article must therefore be hereby marked *advertisement* in accordance with 18 U.S.C. Section 1734 solely to indicate this fact.

Received 11/16/2009; revised 03/25/2010; accepted 04/22/2010; published OnlineFirst 06/08/2010.

References

1. Cantley LC. The phosphoinositide 3-kinase pathway. Science 2002; 296:1655–7.
2. Engelman JA, Luo J, Cantley LC. The evolution of phosphatidylinositol 3-kinases as regulators of growth and metabolism. Nat Rev Genet 2006;7:606–19.
3. Samuels Y, Velculescu VE. Oncogenic mutations of PIK3CA in human cancers. Cell Cycle 2004;3:1221–4.
4. Samuels Y, Wang Z, Bardelli A, et al. High frequency of mutations of the PIK3CA gene in human cancers. Science 2004;304:554.
5. Ma YY, Wei SJ, Lin YC, et al. PIK3CA as an oncogene in cervical cancer. Oncogene 2000;19:2739–44.
6. Shayesteh L, Lu Y, Kuo WL, et al. PIK3CA is implicated as an oncogene in ovarian cancer. Nat Genet 1999;21:99–102.
7. Li J, Yen C, Liaw D, et al. PTEN, a putative protein tyrosine phosphatase gene mutated in human brain, breast, and prostate cancer. Science 1997;275:1943–7.
8. Steck PA, Pershouse MA, Jasser SA, et al. Identification of a candidate tumour suppressor gene, MMAC1, at chromosome 10q23.3 that is mutated in multiple advanced cancers. Nat Genet 1997;15:356–62.
9. Vivanco I, Sawyers CL. The phosphatidylinositol 3-kinase AKT pathway in human cancer. Nat Rev Cancer 2002;2:489–501.
10. Hu L, Zaloudek C, Mills GB, Gray J, Jaffe RB. *In vivo* and *in vitro* ovarian carcinoma growth inhibition by a phosphatidylinositol 3-kinase inhibitor (LY294002). Clin Cancer Res 2000;6:880–6.
11. Ihle NT, Williams R, Chow S, et al. Molecular pharmacology and antitumor activity of PX-866, a novel inhibitor of phosphoinositide-3-kinase signaling. Mol Cancer Ther 2004;3:763–72.
12. Yaguchi S, Fukui Y, Koshimizu I, et al. Antitumor activity of ZSTK474, a new phosphatidylinositol 3-kinase inhibitor. J Natl Cancer Inst 2006;98:545–56.
13. Engelman JA. Targeting PI3K signalling in cancer: opportunities, challenges and limitations. Nat Rev Cancer 2009;9:550–62.
14. Hoeflich KP, O'Brien C, Boyd Z, et al. *In vivo* antitumor activity of MEK and phosphatidylinositol 3-kinase inhibitors in basal-like breast cancer models. Clin Cancer Res 2009;15:4649–64.
15. Kong D, Yamori T. Advances in development of phosphatidylinositol 3-kinase inhibitors. Curr Med Chem 2009;16:2839–54.
16. Ihle NT, Powis G. Take your PIK: phosphatidylinositol 3-kinase inhibitors race through the clinic and toward cancer therapy. Mol Cancer Ther 2009;8:1–9.
17. Knight ZA, Gonzalez B, Feldman ME, et al. A pharmacological map of the PI3-K family defines a role for p110α in insulin signaling. Cell 2006;125:733–47.
18. Liu P, Cheng H, Roberts TM, Zhao JJ. Targeting the phosphoinositide 3-kinase pathway in cancer. Nat Rev Drug Discov 2009;8:627–44.
19. Paez JG, Janne PA, Lee JC, et al. EGFR mutations in lung cancer: correlation with clinical response to gefitinib therapy. Science 2004; 304:1497–500.
20. Lynch TJ, Bell DW, Sordella R, et al. Activating mutations in the epidermal growth factor receptor underlying responsiveness of non-small-cell lung cancer to gefitinib. N Engl J Med 2004;350: 2129–39.
21. Lievre A, Bachet JB, Le Corre D, et al. KRAS mutation status is predictive of response to cetuximab therapy in colorectal cancer. Cancer Res 2006;66:3992–5.
22. Siena S, Sartore-Bianchi A, Di Nicolantonio F, Balfour J, Bardelli A. Biomarkers predicting clinical outcome of epidermal growth factor receptor-targeted therapy in metastatic colorectal cancer. J Natl Cancer Inst 2009;101:1308–24.
23. Engelman JA, Chen L, Tan X, et al. Effective use of PI3K and MEK inhibitors to treat mutant Kras G12D and PIK3CA H1047R murine lung cancers. Nat Med 2008;14:1351–6.
24. Jhawer M, Goel S, Wilson AJ, et al. PIK3CA mutation/PTEN expression status predicts response of colon cancer cells to the epidermal

growth factor receptor inhibitor cetuximab. Cancer Res 2008;68:1953–61.
25. Sartore-Bianchi A, Martini M, Molinari F, et al. PIK3CA mutations in colorectal cancer are associated with clinical resistance to EGFR-targeted monoclonal antibodies. Cancer Res 2009;69:1851–7.
26. Markman B, Atzori F, Perez-Garcia J, Tabernero J, Baselga J. Status of PI3K inhibition and biomarker development in cancer therapeutics. Ann Oncol 2010;21:683–91.
27. Yamori T, Matsunaga A, Sato S, et al. Potent antitumor activity of MS-247, a novel DNA minor groove binder, evaluated by an *in vitro* and *in vivo* human cancer cell line panel. Cancer Res 1999;59:4042–9.
28. Yamori T. Panel of human cancer cell lines provides valuable database for drug discovery and bioinformatics. Cancer Chemother Pharmacol 2003;52 Suppl 1:S74–9.
29. Shoemaker RH. The NCI60 human tumour cell line anticancer drug screen. Nat Rev Cancer 2006;6:813–23.
30. Paull KD, Shoemaker RH, Hodes L, et al. Display and analysis of patterns of differential activity of drugs against human tumor cell lines: development of mean graph and COMPARE algorithm. J Natl Cancer Inst 1989;81:1088–92.
31. Dan S, Tsunoda T, Kitahara O, et al. An integrated database of chemosensitivity to 55 anticancer drugs and gene expression profiles of 39 human cancer cell lines. Cancer Res 2002;62:1139–47.
32. Sugita H, Dan S, Kong D, Tomida A, Yamori T. A new evaluation method for quantifying PI3K activity by HTRF assay. Biochem Biophys Res Commun 2008;377:941–5.
33. Monks A, Scudiero D, Skehan P, et al. Feasibility of a high-flux anticancer drug screen using a diverse panel of cultured human tumor cell lines. J Natl Cancer Inst 1991;83:757–66.
34. Vasudevan KM, Barbie DA, Davies MA, et al. AKT-independent signaling downstream of oncogenic PIK3CA mutations in human cancer. Cancer Cell 2009;16:21–32.
35. Stemke-Hale K, Gonzalez-Angulo AM, Lluch A, et al. An integrative genomic and proteomic analysis of PIK3CA, PTEN, AKT mutations in breast cancer. Cancer Res 2008;68:6084–91.
36. Zimmermann S, Moelling K. Phosphorylation and regulation of Raf by Akt (protein kinase B). Science 1999;286:1741–4.
37. Kong D, Dan S, Yamazaki K, Yamori T. Inhibition profiles of phosphatidylinositol 3-kinase inhibitors against PI3K superfamily and human cancer cell line panel JFCR39. Eur J Cancer 2010;46:1111–21.
38. Raynaud FI, Eccles SA, Patel S, et al. Biological properties of potent inhibitors of class I phosphatidylinositide 3-kinases: from PI-103 through PI-540, PI-620 to the oral agent GDC-0941. Mol Cancer Ther 2009;8:1725–38.
39. Folkes AJ, Ahmadi K, Alderton WK, et al. The identification of 2-(1*H*-indazol-4-yl)-6-(4-methanesulfonyl-piperazin-1-ylmethyl)-4-morpholin-4-yl-t hieno[3,2-*d*]pyrimidine (GDC-0941) as a potent, selective, orally bioavailable inhibitor of class I PI3 kinase for the treatment of cancer. J Med Chem 2008;51:5522–32.
40. Serra V, Markman B, Scaltriti M, et al. NVP-BEZ235, a dual PI3K/mTOR inhibitor, prevents PI3K signaling and inhibits the growth of cancer cells with activating PI3K mutations. Cancer Res 2008;68:8022–30.
41. Brachmann SM, Hofmann I, Schnell C, et al. Specific apoptosis induction by the dual PI3K/mTor inhibitor NVP-BEZ235 in HER2 amplified and PIK3CA mutant breast cancer cells. Proc Natl Acad Sci U S A 2009;106:22299–304.
42. Ihle NT, Lemos R, Jr., Wipf P, et al. Mutations in the phosphatidylinositol-3-kinase pathway predict for antitumor activity of the inhibitor PX-866 whereas oncogenic Ras is a dominant predictor for resistance. Cancer Res 2009;69:143–50.
43. Sarbassov DD, Guertin DA, Ali SM, Sabatini DM. Phosphorylation and regulation of Akt/PKB by the rictor-mTOR complex. Science 2005;307:1098–101.

ELSEVIER

European Journal of Cardio-thoracic Surgery 38 (2010) 498—502

EUROPEAN JOURNAL OF CARDIO-THORACIC SURGERY

www.elsevier.com/locate/ejcts

Prognostic value and significance of subcarinal and superior mediastinal lymph node metastasis in lower lobe tumours

Hirofumi Uehara [a], Yukinori Sakao [a], Mingyon Mun [a], Ken Nakagawa [a], Makoto Nishio [b], Yuichi Ishikawa [c], Sakae Okumura [a,*]

[a] *Department of Thoracic Surgical Oncology, Cancer Institute Hospital, Japanese Foundation for Cancer Research, Tokyo, Japan*
[b] *Department of Thoracic Medical Oncology, Cancer Institute Hospital, Japanese Foundation for Cancer Research, Tokyo, Japan*
[c] *Department of Pathology, Cancer Institute, Japanese Foundation for Cancer Research, Tokyo, Japan*

Received 31 August 2009; received in revised form 3 February 2010; accepted 16 February 2010; Available online 8 April 2010

Abstract

Objective: The new seventh edition of the tumour, node and metastasis (TNM) classification now groups part of the #10 lymph nodes, which include the subcarinal space along with the inferior border of the main-stem bronchus (#10 below), as being a part of the 'subcarinal zone'. In this retrospective study, we aimed to evaluate the clinical significance of including the '#10 below' lymph node with the 'subcarinal zone'. **Methods:** Between 1980 and 2002, the locations of the 66 pN1 and 83 pN2 were found to be part of the bilateral lower lobe in 149 patients. The group comprised 107 males and 42 females, with ages ranging from 16 to 81 years (median: 61.4 years). The clinicopathological records were examined with regard to age, sex, nodal status, T factor and histological type. These variables were analysed as risk factors for superior mediastinal lymph node (SML) metastasis and prognosis. **Results:** Of 149 cases, 28 were #10 below positive/#7 negative (only #10 group), 29 were #10 below negative/#7 positive (only #7 group) and 37 were #10 below positive/#7 positive (double-positive group). There was a significantly higher incidence (64.9%, 24/37) of SML metastasis for the double-positive group as compared to only #10 (14.3%, 4/28) and only #7 groups (31.0%, 9/29) ($P < 0.001$). The overall 5-year survival rates for the only #10, only #7 and the double-positive groups were 50%, 28% and 22%, respectively ($P = 0.02$). **Conclusions:** As compared to #10 metastasis, #7 metastasis is a prognostic risk factor for highly advanced SML metastasis and a poorer prognosis. Therefore, since #10 below and #7 provide different types of diagnostic information, they may not be bundled together during patient evaluations.

Keywords: Lung cancer; Lung cancer surgery; Lung cancer; Diagnosis and staging; Lymph nodes; Outcomes

1. Introduction

Accurate staging of non-small-cell lung cancer (NSCLC) based on the tumour, node and metastasis (TNM) classification is used worldwide. The lung cancer-staging system was first developed in 1973. In 1986, Mountain proposed the current TNM classification [1], with further revisions being made in 1997 [2]. Although this classification has been widely accepted, much debate still persists concerning the exact boundary between the N1 and N2 stations.

The seventh edition of the TNM classification is currently in the process of being revised and it is expected that the 'zone classification' will be adopted for classification of the pN factor [3,4]. During the past few decades, two types of lymph node maps have been proposed, including Naruke's [5] and the American Thoracic Society (MD-ATS) maps [6—8]. Based on the seventh TNM classification, Japanese surgical cases were staged in accordance with the Naruke lymph node map [5], which has been adopted as the official staging map by the Japan Lung Cancer Society [6]. All of the cases from other countries have been staged according to the MD-ATS map [7—9]. With regard to the seventh TNM classification reorganisation, Rusch et al. reported that 'The main discrepancy between these two lymph node maps is that the Naruke map considers lymph nodes in the subcarinal space along the inferior border of the main-stem bronchus (which we will refer to as '#10 below' in the remainder of the text) to be station 10 (hence, N1), whereas in the MD-ATS map, these are labeled as level 7 (and, therefore, N2)' [3,4].

In this retrospective study, we aimed to evaluate the clinical significance of including the '#10 below' lymph node with the 'subcarinal zone'.

* Corresponding author. Address: Department of Thoracic Surgical Oncology, Cancer Institute Hospital, Japanese Foundation for Cancer Research, 3-10-6 Ariake, Koto-ku, Tokyo 135-8550, Japan. Tel.: +81 3 3520 0111; fax: +81 3 3570 0343.
E-mail address: sokumura@jfcr.or.jp (S. Okumura).

1010-7940/$ — see front matter
doi:10.1016/j.ejcts.2010.02.027

2. Materials and methods

As this was a retrospective study and the individual patients were not identifiable, our Institutional Review Board waived the requirement to obtain patient consent.

A total of 1835 cases that underwent pulmonary resection for NSC primary lung cancers between January 1980 and December 2002 were found within the surgical files of the Cancer Institute Hospital, Tokyo, Japan. Of these cases, 1644 met the criteria of the Japanese Lung Cancer Society for curative pulmonary resection [10]. Curative resection was defined as a complete resection of the lung cancer with no evident cancer cells remaining. The absence of cancer cells was based on both surgical and pathological findings.

Staging definitions for T (primary tumour), N (regional lymph nodes) and M (distant metastasis) components were made according to the International Staging System for Lung Cancers [11]. Lymph node involvement was marked using the map of Naruke [5]. Lymph nodes were characterised as being invaded when direct extension or metastases were observed.

In this study, we define 'the nodes at the tracheal bifurcation' as being the #7 lymph node (N2), while 'the nodes around the main-stem bronchi' are defined as being the #10 lymph node (N1) [5,12]. In addition, in #10 lymph node, the node presented at inferior border of the main-stem bronchus as being the #10 below lymph node (N1).

Histopathological studies were conducted according to the World Health Organization (WHO) criteria [13]. There were four surgeons involved in this study. All pulmonary resections and lymph node dissections were performed in the same way.

All patients underwent a preoperative assessment, which included chest X-ray, thoracic and upper abdomen computerised tomography (CT) scan, bone scan, brain magnetic resonance imaging (MRI) or CT, basic blood test and cardiopulmonary evaluation. Mediastinoscopy and positron-emission tomography were not performed in this series.

To evaluate the clinical significance of including the #10 below lymph node in the 'subcarinal zone', we designated the location of the pN1 and pN2 tumours as both being part of the bilateral lower lobe. Therefore, we retrospectively analysed the pattern of lymph node metastasis in 149 out of the total 1644 patients. There were 107 men and 42 women, with a median age of 61.4 years (range: 16–81 years). The prognosis (survival rates) for cases with tumours of the bilateral lower lobe was 66% for patients with pN1 and 83% for patients with pN2. In patients that underwent complete resections, 77 (51.7%) had lobectomies, 46 (30.9%) had bilobectomies and 26 (17.4%) had pneumonectomies. Pathological examinations revealed that there were 32 (21.5%) T1 cases, 54 (36.2%) T2 cases, 12 (8.1%) T3 cases and 51 (34.2%) T4 cases. For the T4 cases, 50 patients had pulmonary metastasis. Using the WHO guidelines to classify the histological types in these patients, we determined that there were 98 adenocarcinomas, 38 squamous cell carcinomas, four large-cell carcinomas and 16 adenosquamous carcinomas. The clinical characteristics for these patients are summarised in Table 1.

The duration of survival in this study was defined as the interval between the date of surgery and the date of death due to any cause over the 5-year postoperative period.

Table 1
Clinicopathological characteristics of patients with pN1 and pN2 lower lobe tumours.

Characteristics	No. of cases
Age (years)	
Mean (range)	61.4 (16-81)
<65/≥65	84/65
Sex	
Male/female	107/42
Tumour location by lobe	
rt lower lobe	87
lt lower lobe	62
Tumour size (mm)	
Mean	40.5
Range	10-140
Operation	
Lobectomy	77
Bilobectomy	46
Pneumonectomy	26
pT Factor	
pT1	32
pT2	54
pT3	12
pT4	51
pN Factor	
pN1	66
pN2	83
#10 below and #7 lymph node	
#10 positive	65
#7 positive	66
PM	
pm0/pm1	99/50
pStage	
IIA	14
IIB	22
IIIA	61
IIIB	52
Pathological type	
Adenocarcinoma	98
Squamous cell carcinoma	38
Large-cell carcinoma	6
Other	7
Total	149

Survival rates from the date of operation were calculated using the Kaplan–Meier life-table method, with the differences in the observed survival rate between the groups tested using the log-rank test. Dichotomous variables are presented as percentages and were compared between groups using a chi-square or Fisher exact test when appropriate. A P-value < 0.05 was considered statistically significant. Statistical analysis was performed with the SPSS analytical software (SPSS Inc., Chicago, IL, USA).

3. Results

3.1. Distribution of lymph node involvement

Of the 149 study subjects, 65 cases (rt:lt = 34:31) had metastasis to the #10 below lymph node and 66 (rt:lt = 44:22)